Rise and Fall, and Slow Rise Again, of Operator Entanglement under Dephasing

D. Wellnitz,[1,2] G. Preisser,[1] V. Alba,[3] J. Dubail,[4,1] and J. Schachenmayer[1,2,*]
[1]ISIS (UMR 7006) and CESQ, CNRS and Université de Strasbourg, 67000 Strasbourg, France
[2]IPCMS (UMR 7504), CNRS, 67000 Strasbourg, France
[3]Dipartimento di Fisica, Università di Pisa, and INFN Sezione di Pisa, Largo Bruno Pontecorvo 3, 56127 Pisa, Italy
[4]Université de Lorraine, CNRS, LPCT, F-54000 Nancy, France

(Received 17 January 2022; accepted 20 September 2022; published 21 October 2022)

The operator space entanglement entropy, or simply "operator entanglement" (OE), is an indicator of the complexity of quantum operators and of their approximability by matrix product operators (MPOs). We study the OE of the density matrix of 1D many-body models undergoing dissipative evolution. It is expected that, after an initial linear growth reminiscent of unitary quench dynamics, the OE should be suppressed by dissipative processes as the system evolves to a simple stationary state. Surprisingly, we find that this scenario breaks down for one of the most fundamental dissipative mechanisms: dephasing. Under dephasing, after the initial "rise and fall," the OE can rise again, increasing logarithmically at long times. Using a combination of MPO simulations for chains of infinite length and analytical arguments valid for strong dephasing, we demonstrate that this growth is inherent to a U(1) conservation law. We argue that in an XXZ spin model and a Bose-Hubbard model the OE grows universally as $\frac{1}{4}\log_2 t$ at long times and as $\frac{1}{2}\log_2 t$ for a Fermi-Hubbard model. We trace this behavior back to anomalous classical diffusion processes.

DOI: 10.1103/PhysRevLett.129.170401

The study of quantum many-body systems through the prism of their quantum entanglement continues to prove extremely fruitful [1,2]. In particular, the growth of entanglement in time-evolving quantum many-body systems is of fundamental interest [3–8]: not only is it useful to characterize the dynamics, but the amount of entanglement also indicates whether a quantum evolution can be efficiently simulated on a classical computer. In one dimension (1D), the connection can be made via the concept of matrix product states (MPSs) [9–12]. An MPS is a decomposition of a many-body state vector into a product of $\chi \times \chi$ matrices (where the entries of the matrices are local kets). In such a representation, the bipartite von Neumann entanglement entropy S is bounded by $\max[S] = \log_2(\chi)$. Consequently, to represent a physical state $|\psi(t)\rangle$ with entanglement entropy $S(t)$ as an MPS, the matrix size (or "bond dimension") has to grow at least as $\chi \propto 2^{S(t)}$ with time. For example, an evolution where S increases linearly in time can therefore be considered computationally hard [13].

The past few years have seen the arrival of novel experiments capable of synthetically engineering quantum many-body models in controllable and clean environments, e.g., using optically trapped ultracold atoms [14–17], molecules [18], or ions [19]. Since such experiments are currently bringing the goal of analog quantum simulation into sight [20,21], the question of entanglement growth, and thus classical simulability, has become very important.

Every experiment has small couplings to its environment and should therefore be considered as an open quantum system described by a density matrix $\hat{\rho}$. Analogously to MPSs for pure states, also a matrix product operator (MPO) form of the density matrix $\hat{\rho}$ can be defined. An MPO form allows one to easily express the density matrix as a Schmidt decomposition between a left and a right block,

$$\hat{\rho} = \sum_a \lambda_a \hat{\tau}_a^{[L]} \hat{\tau}_a^{[R]}, \tag{1}$$

with $\mathrm{Tr}(\hat{\tau}_a^{[L/R]} \hat{\tau}_b^{[L/R]}) = \delta_{ab}$, and λ_a as the Schmidt coefficients [schematically this is depicted in Fig. 1(b)]. The bipartite entropy of this decomposition is given by the operator space entanglement entropy, or simply operator entanglement (OE), defined as [7,22–30]

$$S_{\mathrm{OP}} = -\sum_a \lambda_a^2 \log_2(\lambda_a^2). \tag{2}$$

The OE quantifies how many Schmidt values are at least needed for faithfully approximating decomposition (1), thus indicating the efficiency of an MPO representation [31]. It can be easily computed numerically [25,27,28,32,33] and is amenable to analytical treatment [26,34,35]. We stress that OE is not necessarily connected to genuine quantum entanglement between distinct blocks of spins when $\hat{\rho}$ is a mixed state. Still, it is a crucial quantity, as it puts severe restrictions on the possibility to approximate $\hat{\rho}$ by an MPO. Furthermore, OE can give insights into quantum many-body effects such as quantum chaos and information scrambling [27,29,30].

Here, we analyze the far-from-equilibrium dynamics of the OE, S_{OP}, in open many-body quantum systems. Our models include coherent nearest-neighbor Hamiltonian couplings that compete with incoherent single-particle dephasing [37,47–50] at rate γ [see sketch in Fig. 1(a)]. Under dephasing, fluctuations and coherences can decay toward equilibrium in a universal algebraic and subdiffusive manor [51–54]. We treat dissipation in a Lindblad master equation. Dephasing arises due to a coupling with the environment in which local magnetization is preserved, e.g., for laser driven transitions due to laser-phase fluctuations [55,56] or due to spontaneous photoabsorption of lattice photons in optical lattices [38]. We compute the evolution of S_{OP} for an infinite MPO representation of the full density matrix using an infinite time-evolving block decimation algorithm with reorthogonalization [39].

Surprisingly, we find that, for the magnetization conserving XXZ model and well-defined initial magnetization [see text below Eq. (3) for the definition of our models], the OE exhibits a universal logarithmic growth at long times [see Figs. 1(c) and 1(d)]. An identical universal behavior is also observed for particle number conserving Bose- and Fermi-Hubbard models (see later discussion). Strikingly, as shown in Fig. 1(e), this logarithmic growth breaks down if the symmetry is broken by initial states or for Liouvillians without magnetization conservation (see Supplemental Material [36] for further initial states and nonconserving Lindblad operators). In the latter scenarios, S_{OP} saturates or even vanishes at long times. In this Letter, we explain this behavior by considering symmetry-resolved OE in combination with known results for classical models of interacting particles [57–59].

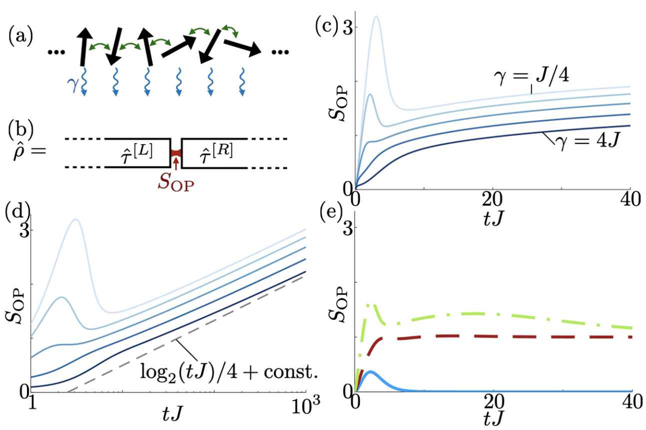

FIG. 1. (a) We compute dynamics of spin chains with coherent nearest-neighbor couplings (double arrows) and local dephasing at rate γ (wiggly arrows). (b) We analyze the growth of OE (S_{OP}) for a bipartition of an infinite chain into a left and right block [from a Schmidt decomposition of the density matrix $\hat\rho$, see Eq. (1)]. (c) Time evolution of S_{OP} for a Néel state in the XXZ model for different values of $\gamma = J/4, J/2, J, 2J$, and $4J$ in order of increasing darkness (anisotropy $J_z = -J$). (d) Same as (c), demonstrating logarithmic growth at long times (log-scale time axis). Gray dashed line, analytic long-time prediction: $S_{\mathrm{OP}} = \log_2(Jt)/4 + \mathrm{const.}$ (e) S_{OP} for dynamics in models breaking magnetization conservation. Green dash-dotted line, XYZ model ($J_x = J, J_y = 0.8J, J_z = -J/2, \gamma = J/2$); red dashed line, transverse field Ising model ($h_z = J, \gamma = J/2$); blue solid line, XXZ model with initial Néel state in x direction ($J_z = -J/2, \gamma = J/2$). Results converged for time step $\Delta tJ = 0.2$ [$\Delta tJ = 0.5$ for (d) at long times] and different values for the bond dimension $\chi = 256$, 512, 1024 (see Supplemental Material [36]).

Model.—We focus on infinite spin-1/2 chains, which evolve under the general Hamiltonian ($\hbar \equiv 1$),

$$\hat H = \frac{1}{4}\sum_i (J_x \hat\sigma_i^x \hat\sigma_{i+1}^x + J_y \hat\sigma_i^y \hat\sigma_{i+1}^y + J_z \hat\sigma_i^z \hat\sigma_{i+1}^z) + \frac{h_z}{2}\sum_i \hat\sigma_i^z. \tag{3}$$

Here, $\hat\sigma_i^{x,y,z}$ denote standard Pauli matrices defined in a local basis $|\downarrow,\uparrow\rangle_i$, $J_{x,y,z}$ are the respective nearest-neighbor spin couplings, and h_z is a field strength along the z direction. Our Hamiltonian (3) includes (i) the XXZ model, with $J_x = J_y \equiv J$, $h_z = 0$, (ii) an XYZ model, with $J_x \equiv J$, $J_x \neq J_y$, and $h_z = 0$, and (iii) a transverse Ising model, with $J_x \equiv J$, $J_y = J_z = 0$, and $h_z \neq 0$. We are interested in the dynamics of highly excited states. Here, we choose pure Néel product states polarized along the z direction, $\hat\rho_0 = |\psi_0\rangle\langle\psi_0|$ with $|\psi_0\rangle = \otimes_i |\uparrow\rangle_{2i-1}|\downarrow\rangle_{2i}$, or a tilted Néel state along the x direction, $|\psi_0\rangle = \otimes_i |\rightarrow\rangle_{2i-1}|\leftarrow\rangle_{2i}$ with $|\leftrightarrows\rangle_i = (|\uparrow\rangle_i \mp |\downarrow\rangle_i)/\sqrt{2}$. Dynamics is governed by a Lindblad master equation,

$$\frac{d}{dt}\hat\rho = -\mathrm{i}[\hat H, \hat\rho] + \sum_i \mathcal{D}^{[i]}\hat\rho \equiv \mathcal{L}\hat\rho, \tag{4}$$

where the local dephasing superoperators are defined as $\mathcal{D}^{[i]}\hat\rho = \gamma/2(\hat\sigma_i^z\hat\rho\hat\sigma_i^z - \hat\rho)$ and $\mathcal{L}$ is the Liouvillian superoperator.

MPO decomposition and OE.—For L spins, the full many-body density matrix $\hat\rho$ of a spin-1/2 system is a $2^L \times 2^L$ Hermitian matrix with unit trace. The amount of information encoded in $\hat\rho$ can be effectively compressed using matrix product decompositions [11,12]. This can be done in different ways [60]: for instance, by decomposing $\hat\rho$ into a particular (not unique) statistical mixture of pure states, while using an MPS for the latter. Then, the Lindblad dynamics can be computed using quantum trajectories [61]. Alternatively, one can use a direct MPO representation for $\hat\rho$, e.g., simply by effectively vectorizing local density matrices [40] or by constructing MPOs in a locally purified form that preserves positivity [62,63].

Here, we decompose $\hat\rho$ into a canonical MPO form [40], which is formally achieved by an iterative application of the Schmidt decomposition from Eq. (1), until each spin n is described by a matrix of unique local operators $\hat\gamma^{[n]}_{a_n,a_{n+1}}$, i.e., $\hat{\rho} = \sum_{\{a_n\}} \prod_n \lambda_{a_n} \hat{\gamma}^{[n]}_{a_n, a_{n+1}}$. By choosing local basis operators $\hat{e}_{i_n}$ for the density matrix of spin n, we can then decompose

$$\hat{\rho} = \sum_{\{i_n\}} \sum_{\{a_n\}}^{\chi} \prod_n \Gamma^{[n] i_n}_{a_n a_{n+1}} \lambda^{[n]}_{a_n} \bigotimes_n \hat{e}_{i_n}, \tag{5}$$

where $\Gamma^{[n]}$ are three-dimensional tensors and $\lambda^{[n]}$ are the Schmidt vectors. Tensors are truncated at a maximum MPO bond dimension χ. All results shown are numerically converged in χ [36]. For $\hat{e}_i$ we choose local eigenoperators for the multiplication with $\hat{\sigma}^z$ from the left and right, to take advantage of the magnetization conservation (see below). Both the initial state and the Hamiltonian are invariant under translation by two lattice sites. As a consequence, in Eq. (5) one has $\Gamma^{[n+2]} = \Gamma^{[n]}$ and $\lambda^{[n+2]} = \lambda^{[n]}$ [39,41], and only two Γ and λ tensors are needed to encode a density matrix. The time evolution is then computed with a fourth-order Trotter decomposition of the matrix exponential of the Liouvillian $\exp(\mathcal{L}\Delta t)$ [39,40,42]. Importantly, since the dynamics is nonunitary, a naive implementation of this algorithm destroys the orthogonality of the decomposition in Eq. (5), such that, with time, the λ's do not correspond to orthogonal Schmidt bases anymore. We fix this by reorthogonalizing the tensors after updates [39].

When considering the XXZ model, the total magnetization $\hat{S}^z = \sum_n \hat{\sigma}^z_n$ is conserved. This means that $\hat{\rho}$ stays an eigenoperator of $\hat{S}^z$ in the sense that $\hat{S}^z \hat{\rho}(t) = M \hat{\rho}(t)$ at all times (for the Néel state, $M = 0$). Note that, alternatively, one could also define a condition for multiplication from the right. Because of magnetization preservation, the $\hat{\tau}^{[R]}_a$ matrices in Eq. (1) can be chosen to be eigenoperators of the "right-half magnetization" of the chain, $\hat{S}^z_R \equiv \sum_{n>0} \hat{\sigma}^z_n$ (without loss of generality, we define the right half as $n > 0$), $\hat{S}^z_R \hat{\tau}^{[R]}_a = M_R \hat{\tau}^{[R]}_a$. Similarly, one can choose $\hat{\tau}^{[L]}_a$ to be eigenoperators of $\hat{S}^z_L \equiv \sum_{n \le 0} \hat{\sigma}^z_n$ with $M_L = -M_R$. This means that the index a in Eq. (1) becomes a composite index $a \to (M_R, a')$, where a' distinguishes the Schmidt coefficients corresponding to the same M_R,

$$\hat{\rho} = \sum_{M_R} \sqrt{p_{M_R}} \sum_{a'} \tilde{\lambda}_{M_R, a'} \hat{\tau}^{[L]}_{-M_R, a'} \hat{\tau}^{[R]}_{M_R, a'}. \tag{6}$$

Here we defined $\tilde{\lambda}_{M_R, a} \equiv \lambda_{M_R, a} / \sqrt{p_{M_R}}$, with $p_{M_R} = \sum_a \lambda^2_{M_R, a}$ as the probability of having magnetization M_R in the right half. The existence of the conservation law makes our simulations much more efficient, since the block-diagonal form of the tensors can be exploited.

Logarithmic increase of OE: Numerical results.—In simulations in Fig. 1, we noticed a distinctive different behavior of OE growth at long times (log growth) for the magnetization conserving XXZ model compared to other models breaking this conservation law. Quite generically, at times $t \ll \gamma^{-1}$, the dynamics is dominated by the Hamiltonian part in Eq. (4). Sufficiently pure states at such short times can be approximated by the state $|\psi_t\rangle = e^{-i\hat{H}t} |\psi_0\rangle$. In that case, the OE is simply twice the entanglement entropy of $|\psi_t\rangle$ (see, e.g., Ref. [26]), and it is well established that the latter generically grows linearly in time (in the absence of disorder). At times $t \gtrsim \gamma^{-1}$, the initial coherence is destroyed by dephasing, and the OE decreases (see Supplemental Material [36] for a more detailed discussion on the parameter dependence of the peak heights). This rise and fall is clearly visible in Fig. 1, and it is typical for OE dynamics, as well as other quantities such as the mutual information [64,65]. Typically, under the dynamics in Eq. (4), the system is expected to relax to a simple stationary state characterized by the conserved quantities of Eq. (4) or to the identity if there is no conservation law. The OE at late times converges toward the OE of that stationary state. This is visible in our simulations of the XYZ and Ising models, see Fig. 1(e). In this case, only the parity $\hat{\Pi} = \otimes_i \hat{\sigma}^z_i$ is preserved by the dynamics. Since the initial Néel state is an eigenstate of $\hat{\Pi}$, the stationary density matrix is a projector on a fixed parity sector, $\frac{1}{2}(1 \pm \hat{\Pi})$, with the $\mathcal{O}(1)$ entropy $S_{\mathrm{OP}} = 1 (= \log_2 2)$. For the XXZ chain with the initial tilted Néel along the x direction, even parity conservation is broken, and the stationary density matrix becomes the identity, $S_{\mathrm{OP}} = 0$. In stark contrast, for the XXZ chain and initial Néel state, after the rise and fall dynamics, the OE increases again at long times, see Fig. 1(c), and this second increase is logarithmic in time, see Fig. 1(d). More precisely, we find the long-time behavior $S_{\mathrm{OP}}(t \to \infty) = \eta \log_2(tJ) + S_0$, which we will also understand analytically below. The prefactor η converges universally to $\eta = 1/4$ independent of the precise values of γ and J_z, as shown in Fig. 2(a), and has also been observed with additional disorder [66]. The offset S_0 depends on the characteristic timescale of the long-time diffusive dynamics set by J, J_z, and γ [36]. Note that we find the evolution of OE in the XXZ model to be independent of the signs of J and J_z.

Mechanism for logarithmic growth: Abelian symmetry and anomalous charge diffusion.—To also analytically understand this behavior, we now consider the XXZ model evolution in the strong dephasing limit $\gamma \gg J$. The dissipators in the master equation (4) project the density matrix onto its diagonal part $\hat{\rho}_{\mathrm{diag}} = \sum_{\boldsymbol{\sigma}} \rho_{\boldsymbol{\sigma}\boldsymbol{\sigma}} |\boldsymbol{\sigma}\rangle\langle\boldsymbol{\sigma}|$, where the $\boldsymbol{\sigma}$ denote all binary vectors of spin-z configurations. The dynamics then reduces to a classical master equation for the probability $p_{\boldsymbol{\sigma}} = \rho_{\boldsymbol{\sigma}\boldsymbol{\sigma}}$, $dp_{\boldsymbol{\sigma}}/dt = \sum_{\boldsymbol{\sigma}'} \mathcal{M}_{\boldsymbol{\sigma}\boldsymbol{\sigma}'} p_{\boldsymbol{\sigma}'}$. The stochastic matrix $\mathcal{M}$ was determined in Ref. [37] in second-order perturbation theory starting from Eq. (4). It takes the form of an effective ferromagnetic Heisenberg Hamiltonian, $\mathcal{M} = -J^2/(8\gamma) \sum_i [\hat{\sigma}^x_i \hat{\sigma}^x_{i+1} + \hat{\sigma}^y_i \hat{\sigma}^y_{i+1} + \hat{\sigma}^z_i \hat{\sigma}^z_{i+1} - 1]$. Importantly, $\mathcal{M}$ is the stochastic matrix of the symmetric simple

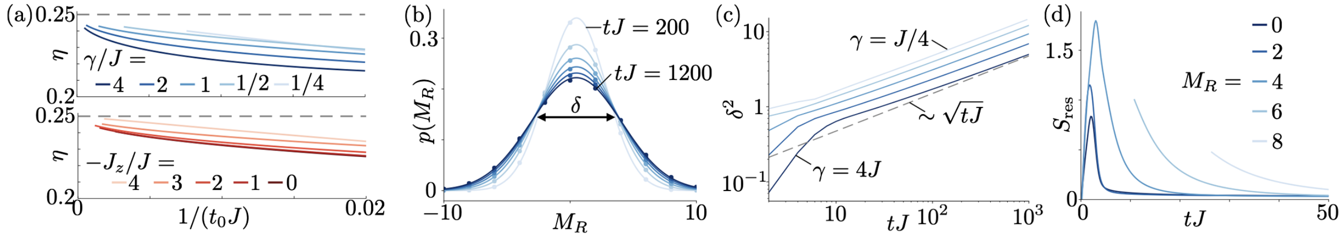

FIG. 2. (a) Numerical determination of η for long times. η at time t_0J is obtained as the local tangent to $S_{\rm OP}(t) = S_0 + \eta \log(tJ)$ at t_0J. We find $\eta \to 1/4$ (gray dashed line) for all parameters and $t_0 \to \infty$. Top (blue): Fixed $J_z = -J$ and various $\gamma/J = 1/4, 1/2, 1, 2, 4$. Bottom (red): Fixed $\gamma = J$ and various $-J_z/J = 0, 1, 2, 3, 4$. (b) Probabilities $p(M_R)$ for right-half magnetization M_R of the infinite chain (see text) at increasingly late times ($200 \le tJ \le 1200$ from light to dark, $J_z = -J, \gamma = J/2$. Lines are Gaussian fits. (c) Variance δ^2 of Gaussian fits [as in (b)] as a function of time for $J_z = -J$ and $\gamma/J = 1/4, 1/2, 1, 2, 4$ (light to dark). The gray dashed line indicates $\delta^2 \sim \sqrt{tJ}$ (double-log scale). (d) Symmetry-resolved operator entanglement entropies $S_{\rm res}$ as a function of time (see text). For short times and the larger $M_R = 6$, 8 the probabilities $p(M_R)$ are exponentially suppressed and no sub-machine-precision data could be extracted. Same parameters as panel (b). Results converged for $\Delta tJ = 0.5$ [(a)-(c)] and $\Delta tJ = 0.1$ [(d)] and different values of $\chi = 512$, 1024, 2048 (see Supplemental Material [36]).

exclusion process (SEP) [43,67], a model of classical hard-core particles that perform random walks.

Crucially, in the SEP, the mean-squared displacement of a tagged particle grows as $\langle X_t^2 \rangle \propto \sqrt{t}$ [58,59,68–71], as opposed to $\propto t$ for a usual random walk. This anomalous diffusion is universally found in problems of so-called single-file diffusion [68,72,73], when classical particles diffuse in one-dimensional channels without bypassing each other. Here, it is now also tied to anomalous scaling of the particle number fluctuations between the left and right half-systems. If $\Delta N(t) = M_R(t)/2$ is the excess number of particles (with respect to the initial Néel state) in the right half-system at time t, and if we tag the particle initially at the origin, then one can estimate $\Delta N(t) \simeq \rho_0 X_t$, where $\rho_0 = 1/2$ is the particle density in the Néel state. Consequently, $\langle \Delta N(t)^2 \rangle \simeq \rho_0^2 \langle X_t^2 \rangle \propto \sqrt{t}$. More generally, the probability distribution of $M_R(t)$ is found to obey a scaling form at long times [69]: $p[M_R(t) = m] \underset{t\to\infty}{\sim} \exp[\sqrt{t} G(m/\sqrt{t})]$. Here, the large-deviation function G is nonpositive, symmetric $[G(u) = G(-u)]$, diverges when $|u| \to \infty$, and has a single minimum at $u = 0$ (see Ref. [69]). In particular, away from the tails, the distribution is Gaussian with standard deviation $\delta = t^{1/4}/\sqrt{|G''(0)|}$. The Shannon entropy associated with number fluctuations is then

$$\begin{aligned} S_{\rm num}(t) &= \sum_{m\in 2\mathbb{Z}} - p(m) \log_2 p(m) \\ &\simeq \int -\sqrt{\frac{2}{\pi\delta^2}} e^{-\frac{m^2}{2\delta^2}} \log_2\left(\sqrt{\frac{2}{\pi\delta^2}} e^{-\frac{m^2}{2\delta^2}}\right) \frac{dm}{2} \\ &= \log_2 \delta + \log_2(\sqrt{\pi e/2}) \underset{t\to\infty}{=} \frac{1}{4}\log_2 t + \mathcal{O}(1). \end{aligned} \quad (7)$$

It is no coincidence that $S_{\rm OP}$ grows in the same way as the number fluctuations $S_{\rm num}$ at long times (see below).

Away from the $\gamma/J \gg 1$ limit, the XXZ chain no longer reduces to the SEP. Nevertheless, we find that the same type of anomalous scaling persists. This is confirmed in Fig. 2, where we show that, for times accessible numerically, $p(M_R = m)$ is approximately Gaussian [Fig. 2(b)] with width $\delta \propto t^{\frac{1}{4}}$ [Fig. 2(c)]. Thus, even though the exact correspondence with the SEP breaks down at finite γ/J, the scaling of $S_{\rm num}$ in Eq. (7) remains unchanged. This result is also consistent with previous studies of transport in the XXZ and related models [74–77].

Symmetry-resolved OE.—We now show how the relation between $S_{\rm OP}$ and $S_{\rm num}$ can be revealed in so-called symmetry-resolved operator entanglement. From Eq. (6) we can derive a decomposition of the OE into the form

$$S_{\rm OP} = \sum_{M_R} p_{M_R} S_{\rm res}(M_R) + S_{\rm num}(p_{M_R}), \quad (8)$$

where the "symmetry-resolved entanglement entropies" are $S_{\rm res}(M_R) = -\sum_a \tilde{\lambda}^2_{M_R,a} \log_2(\tilde{\lambda}^2_{M_R,a})$, and $S_{\rm num}$ is given in Eq. (7). Such symmetry-resolved entropies have attracted attention recently [8,78–82]. In Fig. 2(d) we display $S_{\rm res}(M_R)$ for different values of M_R. Also $S_{\rm res}$ exhibits the rise and fall phenomenon discussed above, but independent of M_R they decrease to very small values at late times. This means that the logarithmic increase $S_{\rm OP}$ is solely due to the growth of $S_{\rm num}$.

Fermi- and Bose-Hubbard models.—To demonstrate the generality of the logarithmic OE growth, we discuss two additional paradigmatic many-body setups featuring number conservation: (i) a Fermi-Hubbard (FH) model, $\hat{H}_{\rm FH} = -J_f \sum_{n,\sigma}(\hat{c}^\dagger_{\sigma,n}\hat{c}_{\sigma,n+1} + {\rm H.c.}) + U_f \sum_n \hat{c}^\dagger_{\uparrow,n}\hat{c}^\dagger_{\downarrow,n}\hat{c}_{\uparrow,n}\hat{c}_{\downarrow,n}$ with creation operators for spin-full fermions on site n, $\hat{c}^\dagger_{\sigma,n}$ ($\sigma = \uparrow, \downarrow$), and (ii) a Bose-Hubbard (BH) model, $\hat{H}_{\rm BH} = -J_b \sum_n (\hat{b}^\dagger_n \hat{b}_{n+1} + {\rm H.c.}) + U_b/2 \sum_n \hat{b}^\dagger_n \hat{b}^\dagger_n \hat{b}_n \hat{b}_n$, for bosons created by $\hat{b}^\dagger_n$. In both cases, we consider dephasing

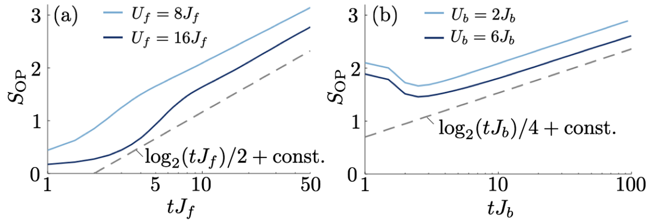

FIG. 3. Logarithmic OE growth in the (a) Fermi-Hubbard and (b) Bose-Hubbard models with dephasing for different interaction strengths $U_{f/b}$. The gray dashed lines indicate the analytically expected long-time growth [36]. The initial states are as follows: (a) one fermion per site with alternating spins $|\cdots\uparrow\downarrow\uparrow\cdots\rangle$ and (b) alternating sites with 0 or 1 boson $|\cdots 101\cdots\rangle$. Parameters: (a) $\gamma_f = 8J_f$ and (b) $\gamma_b = 2J_b$, $\chi = 512,\ 256$, $\Delta t J_{f/b} = 1/2$, maximum bosons per site $n_{\max} = 4$.

$\mathcal{D}^{[k]}\hat{\rho} = \gamma\hat{L}_k\hat{\rho}\hat{L}_k^\dagger - \gamma(\hat{L}_k^\dagger\hat{L}_k\hat{\rho} + \hat{\rho}\hat{L}_k^\dagger\hat{L}_k)/2$, where $\hat{L}_{\sigma,n} = \hat{c}_{\sigma,n}^\dagger\hat{c}_{\sigma,n}$ and $\hat{L}_n = \hat{b}_n^\dagger\hat{b}_n$ in the FH and BH case, respectively. As demonstrated in Fig. 3, both models also exhibit a long-time logarithmic OE growth. In the FH model, we observe $S_{\mathrm{OP}} \sim \log_2(tJ_f)/2$. For $\gamma \gg J_f, U_f$, this can be understood analytically by considering the FH chain as the sum of two chains, one for each spin degree of freedom, both of which are described by the SEP and exhibit $S_{\mathrm{OP}} \sim \log_2(tJ_f)/4$. Here, interactions contribute only at higher orders (see Supplemental Material [36]). The BH model exhibits $S_{\mathrm{OP}} \sim \log_2(tJ_b)/4$ analogous to the XXZ model. For large $U_b \gg \gamma \gg J_b$, the creation of doublons is energetically suppressed, leading back to the SEP. For finite interaction strength ($\gamma \gg J_b, U_b$), a different classical limit is reached, which also features logarithmic OE growth with a prefactor close to $1/4$ stemming from a "symmetric inclusion process" [36,43].

Conclusion.—We showed that, in a dissipative system possessing a U(1) conservation law, the operator entanglement grows logarithmically at long times. We pinpointed the mechanism that leads to this logarithmic growth and identified its prefactor with the (possibly anomalous) exponent characterizing the fluctuations of the charge associated with the U(1) symmetry. Our results and methods are of general interest to studies of imperfect quantum computation and quantum simulation platforms, currently pushing into a regime where they may offer a quantum advantage. The entanglement entropy dynamics we study here connects directly to similar results obtained for discrete quantum circuit models [27,32,83,84] or to other dissipative simulation methods such as quantum trajectories [85,86]. An understanding of the destructive processes of the environment on dynamics are essential, and the interplay between dissipation and coherent couplings can lead to interesting physics or state engineering (e.g., [87–90]). In the future, it will be interesting to investigate how the presence of more complex symmetries such as SU(N) impacts entanglement dynamics.

We thank P. Calabrese, O. Castro-Alvaredo, A. Grabsch, G. Misguich, S. Murciano, G. Pupillo, and G. Schütz for helpful discussions. This work was supported by LabEx NIE, under Contract No. ANR-11-LABX0058 NIE, and the QUSTEC program, which has received funding from the European Union's Horizon 2020 research and innovation program under the Marie Skłodowska-Curie Grant Agreement No. 847471. This work is part of the Interdisciplinary Thematic Institute QMat, as part of the ITI 2021-2028 program of the University of Strasbourg, CNRS and Inserm, and was supported by IdEx Unistra (ANR-10-IDEX-0002), SFRI STRAT'US project (ANR-20-SFRI-0012), and EUR QMAT ANR-17-EURE-0024 under the framework of the French Investments for the Future Program. Our MPO codes make use of the intelligent tensor library (ITensor) [91]. Computations were carried out using resources of the High Performance Computing Center of the University of Strasbourg, funded by Equip@Meso (as part of the Investments for the Future Program) and CPER Alsacalcul/Big Data.

*schachenmayer@unistra.fr

[1] L. Amico, R. Fazio, A. Osterloh, and V. Vedral, Entanglement in many-body systems, Rev. Mod. Phys. **80**, 517 (2008).

[2] J. Eisert, M. Cramer, and M. B. Plenio, Colloquium: Area laws for the entanglement entropy, Rev. Mod. Phys. **82**, 277 (2010).

[3] P. Calabrese and J. Cardy, Evolution of entanglement entropy in one-dimensional systems, J. Stat. Mech. (2005) P04010.

[4] M. Fagotti and P. Calabrese, Evolution of entanglement entropy following a quantum quench: Analytic results for the xy chain in a transverse magnetic field, Phys. Rev. A **78**, 010306(R) (2008).

[5] M. Žnidarič, T. Prosen, and P. Prelovšek, Many-body localization in the Heisenberg XXZ magnet in a random field, Phys. Rev. B **77**, 064426 (2008).

[6] V. Alba and P. Calabrese, Entanglement and thermodynamics after a quantum quench in integrable systems, Proc. Natl. Acad. Sci. U.S.A. **114**, 7947 (2017).

[7] C. Jonay, D. A. Huse, and A. Nahum, Coarse-grained dynamics of operator and state entanglement, arXiv:1803.00089.

[8] A. Lukin, M. Rispoli, R. Schittko, M. E. Tai, A. M. Kaufman, S. Choi, V. Khemani, J. Léonard, and M. Greiner, Probing entanglement in a many-body–localized system, Science **364**, 256 (2019).

[9] G. Vidal, Efficient Simulation of One-Dimensional Quantum Many-Body Systems, Phys. Rev. Lett. **93**, 040502 (2004).

[10] F. Verstraete, V. Murg, and J. I. Cirac, Matrix product states, projected entangled pair states, and variational renormalization group methods for quantum spin systems, Adv. Phys. **57**, 143 (2008).

[11] U. Schollwöck, The density-matrix renormalization group in the age of matrix product states, Ann. Phys. (Amsterdam) **326**, 96 (2011).

[12] S. Paeckel, T. Köhler, A. Swoboda, S. R. Manmana, U. Schollwöck, and C. Hubig, Time-evolution methods for matrix-product states, Ann. Phys. (Amsterdam) **411**, 167998 (2019).

[13] N. Schuch, M. M. Wolf, F. Verstraete, and J. I. Cirac, Entropy Scaling and Simulability by Matrix Product States, Phys. Rev. Lett. **100**, 030504 (2008).

[14] I. Bloch, J. Dalibard, and S. Nascimbène, Quantum simulations with ultracold quantum gases, Nat. Phys. **8**, 267 (2012).

[15] C. S. Adams, J. D. Pritchard, and J. P. Shaffer, Rydberg atom quantum technologies, J. Phys. B **53**, 012002 (2019).

[16] A. Browaeys and T. Lahaye, Many-body physics with individually controlled Rydberg atoms, Nat. Phys. **16**, 132 (2020).

[17] M. Morgado and S. Whitlock, Quantum simulation and computing with Rydberg-interacting qubits, AVS Quantum Sci. **3**, 023501 (2021).

[18] B. Gadway and B. Yan, Strongly interacting ultracold polar molecules, J. Phys. B **49**, 152002 (2016).

[19] R. Blatt and C. F. Roos, Quantum simulations with trapped ions, Nat. Phys. **8**, 277 (2012).

[20] J. I. Cirac and P. Zoller, Goals and opportunities in quantum simulation, Nat. Phys. **8**, 264 (2012).

[21] I. M. Georgescu, S. Ashhab, and F. Nori, Quantum simulation, Rev. Mod. Phys. **86**, 153 (2014).

[22] P. Zanardi, C. Zalka, and L. Faoro, Entangling power of quantum evolutions, Phys. Rev. A **62**, 030301(R) (2000).

[23] P. Zanardi, Entanglement of quantum evolutions, Phys. Rev. A **63**, 040304(R) (2001).

[24] X. Wang and P. Zanardi, Quantum entanglement of unitary operators on bipartite systems, Phys. Rev. A **66**, 044303 (2002).

[25] T. Prosen and I. Pižorn, Operator space entanglement entropy in a transverse Ising chain, Phys. Rev. A **76**, 032316 (2007).

[26] J. Dubail, Entanglement scaling of operators: A conformal field theory approach, with a glimpse of simulability of long-time dynamics in $1+1$d, J. Phys. A **50**, 234001 (2017).

[27] T. Zhou and D. J. Luitz, Operator entanglement entropy of the time evolution operator in chaotic systems, Phys. Rev. B **95**, 094206 (2017).

[28] V. Alba, J. Dubail, and M. Medenjak, Operator Entanglement in Interacting Integrable Quantum Systems: The Case of the Rule 54 Chain, Phys. Rev. Lett. **122**, 250603 (2019).

[29] H. Wang and T. Zhou, Barrier from chaos: Operator entanglement dynamics of the reduced density matrix, J. High Energy Phys. 12 (2019) 001.

[30] G. Styliaris, N. Anand, and P. Zanardi, Information Scrambling over Bipartitions: Equilibration, Entropy Production, and Typicality, Phys. Rev. Lett. **126**, 030601 (2021).

[31] Note that here this indicates approximability with respect to the two-norm of the vectorized density matrix.

[32] K. Noh, L. Jiang, and B. Fefferman, Efficient classical simulation of noisy random quantum circuits in one dimension, Quantum **4**, 318 (2020).

[33] T. Rakovszky, C. W. von Keyserlingk, and F. Pollmann, Dissipation-assisted operator evolution method for capturing hydrodynamic transport, Phys. Rev. B **105**, 075131 (2022).

[34] B. Bertini, P. Kos, and T. Prosen, Operator entanglement in local quantum circuits I: Chaotic dual-unitary circuits, SciPost Phys. **8**, 067 (2020).

[35] B. Bertini, P. Kos, and T. Prosen, Operator entanglement in local quantum circuits II: Solitons in chains of qubits, SciPost Phys. **8**, 068 (2020).

[36] See Supplemental Material at http://link.aps.org/supplemental/10.1103/PhysRevLett.129.170401 for details on the MPO simulations, nonconserving models, the perturbative OE offset, for numerical results on the parameter dependence of the short-time peaks, and for analytical results for the Hubbard models, including Refs. [37–46].

[37] Z. Cai and T. Barthel, Algebraic versus Exponential Decoherence in Dissipative Many-Particle Systems, Phys. Rev. Lett. **111**, 150403 (2013).

[38] H. Pichler, A. J. Daley, and P. Zoller, Nonequilibrium dynamics of bosonic atoms in optical lattices: Decoherence of many-body states due to spontaneous emission, Phys. Rev. A **82**, 063605 (2010).

[39] R. Orús and G. Vidal, Infinite time-evolving block decimation algorithm beyond unitary evolution, Phys. Rev. B **78**, 155117 (2008).

[40] M. Zwolak and G. Vidal, Mixed-State Dynamics in One-Dimensional Quantum Lattice Systems: A Time-Dependent Superoperator Renormalization Algorithm, Phys. Rev. Lett. **93**, 207205 (2004).

[41] G. Vidal, Classical Simulation of Infinite-Size Quantum Lattice Systems in One Spatial Dimension, Phys. Rev. Lett. **98**, 070201 (2007).

[42] A. T. Sornborger and E. D. Stewart, Higher-order methods for simulations on quantum computers, Phys. Rev. A **60**, 1956 (1999).

[43] D. Bernard, T. Jin, and O. Shpielberg, Transport in quantum chains under strong monitoring, Europhys. Lett. **121**, 60006 (2018).

[44] C. Giardina, F. Redig, and K. Vafayi, Correlation inequalities for interacting particle systems with duality, J. Stat. Phys. **141**, 242 (2010).

[45] S. Grosskinsky, F. Redig, and K. Vafayi, Dynamics of condensation in the symmetric inclusion process, Electron. J. Pro **18**, 1 (2013).

[46] R. G. Miller, The jackknife–a review, Biometrika **61**, 1 (1974).

[47] D. Rossini and E. Vicari, Coherent and dissipative dynamics at quantum phase transitions, Phys. Rep. **936**, 1 (2021).

[48] M. V. Medvedyeva, F. H. L. Essler, and T. Prosen, Exact Bethe Ansatz Spectrum of a Tight-Binding Chain with Dephasing Noise, Phys. Rev. Lett. **117**, 137202 (2016).

[49] M. Foss-Feig, J. T. Young, V. V. Albert, A. V. Gorshkov, and M. F. Maghrebi, Solvable Family of Driven-Dissipative

Many-Body Systems, Phys. Rev. Lett. **119**, 190402 (2017).
[50] M. Žnidarič, Relaxation times of dissipative many-body quantum systems, Phys. Rev. E **92**, 042143 (2015).
[51] D. Poletti, J.-S. Bernier, A. Georges, and C. Kollath, Interaction-Induced Impeding of Decoherence and Anomalous Diffusion, Phys. Rev. Lett. **109**, 045302 (2012).
[52] D. Poletti, P. Barmettler, A. Georges, and C. Kollath, Emergence of Glasslike Dynamics for Dissipative and Strongly Interacting Bosons, Phys. Rev. Lett. **111**, 195301 (2013).
[53] J. Ren, Q. Li, W. Li, Z. Cai, and X. Wang, Noise-Driven Universal Dynamics towards an Infinite Temperature State, Phys. Rev. Lett. **124**, 130602 (2020).
[54] R. Bouganne, M. Bosch Aguilera, A. Ghermaoui, J. Beugnon, and F. Gerbier, Anomalous decay of coherence in a dissipative many-body system, Nat. Phys. **16**, 21 (2020).
[55] D. Plankensteiner, J. Schachenmayer, H. Ritsch, and C. Genes, Laser noise imposed limitations of ensemble quantum metrology, J. Phys. B **49**, 245501 (2016).
[56] C. W. Gardiner and P. Zoller, *Quantum Noise* (Springer, New York, 1991), Chap. 3.6, p. 77.
[57] T. E. Harris, Diffusion with "collisions" between particles, J. Appl. Probab. **2**, 323 (1965).
[58] D. G. Levitt, Dynamics of a single-file pore: Non-Fickian behavior, Phys. Rev. A **8**, 3050 (1973).
[59] R. Arratia, The motion of a tagged particle in the simple symmetric exclusion system on *Z*, Ann. Probab. **11**, 362 (1983).
[60] H. Weimer, A. Kshetrimayum, and R. Orús, Simulation methods for open quantum many-body systems, Rev. Mod. Phys. **93**, 015008 (2021).
[61] A. J. Daley, Quantum trajectories and open many-body quantum systems, Adv. Phys. **63**, 77 (2014).
[62] F. Verstraete, J. J. García-Ripoll, and J. I. Cirac, Matrix Product Density Operators: Simulation of Finite-Temperature and Dissipative Systems, Phys. Rev. Lett. **93**, 207204 (2004).
[63] A. H. Werner, D. Jaschke, P. Silvi, M. Kliesch, T. Calarco, J. Eisert, and S. Montangero, Positive Tensor Network Approach for Simulating Open Quantum Many-Body Systems, Phys. Rev. Lett. **116**, 237201 (2016).
[64] F. Carollo and V. Alba, Dissipative quasiparticle picture for quadratic Markovian open quantum systems, Phys. Rev. B **105**, 144305 (2022).
[65] V. Alba and F. Carollo, Hydrodynamics of quantum entropies in Ising chains with linear dissipation, J. Phys. A **55**, 074002 (2022).
[66] M. V. Medvedyeva, T. Prosen, and M. Žnidarič, Influence of dephasing on many-body localization, Phys. Rev. B **93**, 094205 (2016).
[67] K. Mallick, The exclusion process: A paradigm for non-equilibrium behaviour, Physica (Amsterdam) **418A**, 17 (2015).
[68] B. Lin, M. Meron, B. Cui, S. A. Rice, and H. Diamant, From Random Walk to Single-File Diffusion, Phys. Rev. Lett. **94**, 216001 (2005).
[69] B. Derrida and A. Gerschenfeld, Current fluctuations of the one dimensional symmetric simple exclusion process with step initial condition, J. Stat. Phys. **136**, 1 (2009).
[70] T. Imamura, K. Mallick, and T. Sasamoto, Large Deviations of a Tracer in the Symmetric Exclusion Process, Phys. Rev. Lett. **118**, 160601 (2017).
[71] A. Grabsch, A. Poncet, P. Rizkallah, P. Illien, and O. Bénichou, Exact closure and solution for spatial correlations in single-file diffusion, Sci. Adv. **8** eabm5043 (2022).
[72] K. Hahn, J. Kärger, and V. Kukla, Single-File Diffusion Observation, Phys. Rev. Lett. **76**, 2762 (1996).
[73] Q.-H. Wei, C. Bechinger, and P. Leiderer, Single-file diffusion of colloids in one-dimensional channels, Science **287**, 625 (2000).
[74] M. Žnidarič, Dephasing-induced diffusive transport in the anisotropic Heisenberg model, New J. Phys. **12**, 043001 (2010).
[75] M. Žnidarič, Exact solution for a diffusive nonequilibrium steady state of an open quantum, J. Stat. Mech. (2010) L05002.
[76] V. Eisler, Crossover between ballistic and diffusive transport: The quantum exclusion process, J. Stat. Mech. (2011) P06007.
[77] J. De Nardis, S. Gopalakrishnan, R. Vasseur, and B. Ware, Subdiffusive hydrodynamics of nearly-integrable anisotropic spin chains, Proc. Natl. Acad. Sci. U.S.A. **119**, e2202823119 (2022).
[78] M. Goldstein and E. Sela, Symmetry-Resolved Entanglement in Many-Body Systems, Phys. Rev. Lett. **120**, 200602 (2018).
[79] J. C. Xavier, F. C. Alcaraz, and G. Sierra, Equipartition of the entanglement entropy, Phys. Rev. B **98**, 041106(R) (2018).
[80] G. Parez, R. Bonsignori, and P. Calabrese, Quasiparticle dynamics of symmetry-resolved entanglement after a quench: Examples of conformal field theories and free fermions, Phys. Rev. B **103**, L041104 (2021).
[81] H. Barghathi, C. M. Herdman, and A. Del Maestro, Rényi Generalization of the Accessible Entanglement Entropy, Phys. Rev. Lett. **121**, 150501 (2018).
[82] H. Barghathi, E. Casiano-Diaz, and A. Del Maestro, Operationally accessible entanglement of one-dimensional spinless fermions, Phys. Rev. A **100**, 022324 (2019).
[83] Y. Li, X. Chen, and M. P. A. Fisher, Quantum Zeno effect and the many-body entanglement transition, Phys. Rev. B **98**, 205136 (2018).
[84] A. Chan, R. M. Nandkishore, M. Pretko, and G. Smith, Unitary-projective entanglement dynamics, Phys. Rev. B **99**, 224307 (2019).
[85] M. Coppola, E. Tirrito, D. Karevski, and M. Collura, Growth of entanglement entropy under local projective measurements, Phys. Rev. B **105**, 094303 (2022).
[86] T. Botzung, S. Diehl, and M. Müller, Engineered dissipation induced entanglement transition in quantum spin chains: From logarithmic growth to area law, Phys. Rev. B **104**, 184422 (2021).
[87] M. J. Mark, S. Flannigan, F. Meinert, J. P. D'Incao, A. J. Daley, and H.-C. Nägerl, Interplay between coherent and dissipative dynamics of bosonic doublons in an optical lattice, Phys. Rev. Res. **2**, 043050 (2020).
[88] B. Zhu, B. Gadway, M. Foss-Feig, J. Schachenmayer, M. L. Wall, K. R. A. Hazzard, B. Yan, S. A. Moses, J. P. Covey,

D. S. Jin, J. Ye, M. Holland, and A. M. Rey, Suppressing the Loss of Ultracold Molecules Via the Continuous Quantum Zeno Effect, Phys. Rev. Lett. **112**, 070404 (2014).

[89] V. S. Shchesnovich and V. V. Konotop, Control of a Bose-Einstein condensate by dissipation: Nonlinear Zeno effect, Phys. Rev. A **81**, 053611 (2010).

[90] T. Müller, S. Diehl, and M. Buchhold, Measurement-Induced Dark State Phase Transitions in Long-Ranged Fermion Systems, Phys. Rev. Lett. **128**, 010605 (2022).

[91] M. Fishman, S. R. White, and E. M. Stoudenmire, The ITensor software library for tensor network calculations, arXiv:2007.14822.